Int. J. Microgravity Sci. Appl., 33 (4) (2016) 330404
DOI: 10.15011//jasma.33.330404

IIIII ISPS-6 Proceedings IIIII
(Original Paper)

Electrochemical Deposition of Binary Alloys: Effect of Gravity on Composition, Morphology and Dendritic Growth

Lok-kun TSUI, Marcel MIBUS, Begum UNVEROGLU and Giovanni ZANGARI

Abstract

In order to better understand alloy electrodeposition processes, it is essential to isolate the various phenomena involved in film formation. One important aspect in this context is the natural convection occurring in electrochemical cells, observed in the presence of gravity and due to the change in electrolyte density upon electrode reactions. These convection patterns can be minimized by the use of horizontal electrodes, with the cathode on top and facing down. Using this geometry and comparing with a number of other cell configurations, we have observed that the suppression of natural convection leads to more uniform nucleation and tighter composition distribution in Cu-Zn-Sn ternary alloy films. Experiments in a flat cell on alloy dendrite growth show that the most stable growth is again in the top cathode configuration; alloying Ag or Ni with Cu leads to more dense dendrites, increase in tip splitting occurrence and in some cases to the destabilization of dendrite formation, leading to dense and compact films.

Keyword(s): Electrodeposition, Films, Coatings, Alloys, Microgravity
Received 29 January 2016, accepted 10 August 2016, published 31 October 2016.

1. Introduction

Electrodeposition of thin films and metallic coatings involves the electrochemical reduction of metal ion precursors from a suitable solvent, most commonly water, onto a conductive electrode acting as a substrate[1,2]. The coated electrode could be directly used for functional applications, or the coating could be removed and utilized elsewhere. Film growth occurs only at conductive regions of the substrates, leading to selective deposition; this feature positions the electrodeposition method in sharp contrast with most physical deposition processes, which mainly form blanket films on a substrate. Another feature of electrodeposition is the diffusional nature of the ionic flow, which leads to relatively uniform coatings also on non-planar substrates. These two features, together with others, discussed for example in Ref.3), lead to unusual capabilities and therefore unique synthetic opportunities for this deposition method.

Today, electrodeposition is widely used to form films, micro- and nanostructures for a variety of advanced functional applications, spanning from electronics, to magnetics, sensing and energy conversion[4]. The ever-growing need for improved performance in devices utilizing metallic materials calls for the increased usage of alloys instead of pure metals, since they provide an enhancement, but most importantly tailoring, of the relevant properties, which is usually achieved by close control of the composition and the micro/nanostructure. This requires in turn an ever-improving control over the deposition process, in particular close monitoring and prediction of compositional variations throughout the film surface and thickness, morphology and thickness distribution. One of the main reasons for composition and morphology variations in electrodeposited films is the dominance of diffusion and convection, which determine the rate of arrival of ions at the electrode. Analytical methods such as the rotating disk electrode (RDE) are available to impose and predict precisely the ion arrival rates at the electrode[5]; conventional electrochemical processes however cannot in most cases utilize these methods and therefore are strongly affected by buoyancy-induced flow, difficult to model and quantify. The effect of natural convection in a conventional electrochemical cell with vertical electrodes facing each other is shown by a computational result reproduced in **Fig. 1**[6]; in electrodeposition the density of the electrolyte at the cathode decreases over time, inducing a vertical flow of the electrolyte at the cathode, resulting in rolling convection between the cathode and anode.

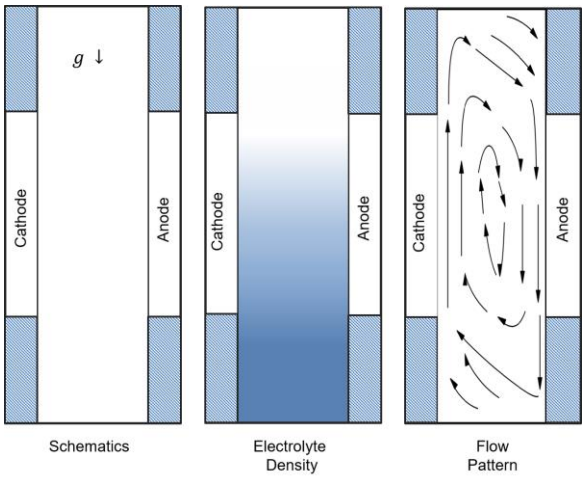

Fig. 1 Flow patterns in a vertical cell during metal plating.

Department of Materials Science & Engineering, University of Virginia, PO Box 400745, 395 McCormick Road, Charlottesville VA22904, USA.
(E-mail: gz3e@virginia.edu)

Electrochemical reactors for microelectronics applications, which handle today 300 mm diameter Silicon wafers, are designed with the surface to be plated on top, facing down; additionally, buoyancy-induced convection is minimized by imposing a forced flow via the judicious placement of several electrolyte jets in the cell.

It is of fundamental interest however to better understand the effect of gravity during electrodeposition processes. Steps forward have been taken by performing experiments in low gravity conditions using parabolic flights and drop towers[7,8]; in particular, in the 1980s NASA researchers performed aircraft parabolic flights, demonstrating the practical absence of natural convection under 10^{-2} g gravity levels and showing also differences in the morphology of electroplates as well as increased corrosion resistance[9,10]. Ground based 2-dimensional cell geometries have also demonstrated to avoid to a large extent the buoyancy-induced flow, despite the fact that they cannot hinder completely convection processes. In particular, it was shown that little differences could be observed between experiments conducted in convection-free bench tests and low gravity experiments in parabolic flights. A suitable geometry to approximate the absence of gravity in a 2-D cell is a configuration with the cathode on top, facing down, with the 3rd dimension being less than 1 mm and ideally few 10s of microns[11].

While extensive experiments have been performed to study the growth and properties of metal films made under low gravity conditions, little attention has been devoted to the electrochemical growth of alloys in low gravity. Considering the need for improved methods for electrochemical alloy synthesis discussed above, it is important to first understand the differences in metal and alloy electrodeposition, and then perform experiments to achieve better insight on gravity effects in electrochemical alloys. In this paper we will therefore provide first a short tutorial on the electrodeposition of alloys, including methods to control and predict composition and microstructure. We will also discuss the use of a horizontal, top cathode cell to minimize buoyancy-induced flow, allowing studies of the growth behavior of alloy films in the virtual absence of convection. Results will be focused on the effect of gravity on nucleation, compositional distribution, and studies of the dendritic growth in binary and ternary electrolytes.

2. Electrodeposition of Alloys

The fundamental laws of metal and alloy electrodeposition have been understood in terms of classical concepts of thermodynamic and kinetics[12]. Briefly, the Nernst equation determines the equilibrium redox potential for the reaction

$$Me^{z+} + ze = Me_{xtal} \quad (1)$$

where Me^{z+} represents the metal ion in solution, z the number of electrons exchanged, e the electron provided by the external circuit, and Me_{xtal} the metal atom placed in a crystallographic position. The corresponding equation for the equilibrium potential E_{eq} is

$$E_{eq}\,(Me^{z+}/Me_{xtal}) = E^0 + (RT/zF)\times\ln(a_{Mez+}) \quad (2)$$

with E^0 the standard electrode potential, R the gas constant, T the absolute temperature, F the Faraday constant, and a_{Mez+} the activity of the metal ion in solution. An externally applied potential E_{app} results in a phase transformation: if $E_{app} > E_{eq}$ the metal oxidizes or dissolves in the electrolyte, while if $E_{app} < E_{eq}$ the metal ion is reduced to a metallic form at the substrate. The driving force for the metal film formation is the overpotential:

$$\eta = E_{appl} - E_{eq} \quad (3)$$

The rate of oxidation or reduction for the metal ion is given, but only for a one electron transfer reaction, by the Butler-Volmer relationship, whereby the current density j is

$$j = j_0\cdot[\exp(-\alpha f\eta) - \exp((1-\alpha)f\eta)] \quad (4)$$

where j_0 is the *exchange current*, that is the rate of the two partial reduction and oxidation reactions under conditions of dynamic equilibrium, when $\eta = 0$. The first term in parenthesis is positive and quantifies the rate of the cathodic reaction, the second the oxidation rate. α represents the symmetry of the energy barrier for the electron exchange and is between 0 and 1, often close to ½; f = F/RT=1/0.0257 V at 298 K. The B-V equation can be often simplified by dropping one of the exponentials; under reduction, i.e. film deposition conditions, therefore $j = j_0\cdot[\exp(-\alpha f\eta)]$.

The kinetics of more complex reduction reactions is determined by their mechanism; it is not possible in general to provide an explicit expression unless the mechanism is known. In practice, an experimental approach is preferred, whereby the deposition kinetics and its mechanism could be determined by measuring the partial currents while varying the concentration of the reactants, including the solution pH[13].

The simplest model of alloy electrodeposition for an alloy M-N assumes that the partial reduction of M and N is unchanged with respect to each metal being deposited alone. Under this Independent Reduction Kinetics (IRK) assumption[14], the current for alloy deposition is the sum of the partial currents and therefore the alloy composition can be determined by experiments that measure the partial currents, for example the composition as a function of applied potential. In general, this IRK assumption does not hold, due to interactions occurring between the two metal ion species. Such interactions may occur (i) in the bulk of the electrolyte, where the presence of N may affect the degree and nature of complexation for M or vice versa; (ii) at the electrode/electrolyte interface, where the presence of intermediate species may affect the relative degree of adsorption and therefore the relative rate of successive reduction steps, and

(iii) at the stage of crystal structure formation, where the interatomic interactions in the solid state would affect the bonding strength and therefore the redox potential of each species. The latter effect can be accounted for under a thermodynamic approximation of the process, which is however valid only under the assumption of negligible deposition overvoltage. This effect has been validated for a variety of alloys and the corresponding phenomenon of underpotential co-deposition is discussed in various pa-pers and a review[15].

In addition, a comprehensive description of alloy electrodeposition requires to take into account ion transport phenomena, in particular hydrodynamic convection and diffusion. Most electrochemical cells are designed with vertically oriented electrodes and operate under spontaneous or forced convection. In both cases the convection patterns may be calculated, but the calculation must be time-dependent and take into account a series of moving boundaries. In particular, buoyancy-driven convective flow is generated during electrodeposition due to gravity effects generated by density gradients. Some commercial electrochemical cells avoid these uncertainties by using forced electrolyte flow; on the other hand, methods that are often used to simulate the absence of gravity is to use thin cells, high viscosity electrolytes, or horizontal electrode configurations with the cathode on top. The latter cell has been extensively used to simulate the absence of gravity, even if convective motion may still arise due to inhomogeneous current density distribution. The study of alloy electrodeposition in this configuration has not been undetaken so far to our knowledge. This paper reports the effect of cell geometry on alloy deposition, focusing on the uniformity of composition, nucleation features, and morphology of dendritic growth.

3. Experimental Details

3.1 Morphological and Compositional Studies of Electroplated Cu-Zn-Sn Alloys

Figure 2 schematically shows the two electrochemical cell geometries utilized to grow Cu-Zn-Sn alloys. Electrodeposition was carried out in a three-electrode configuration using a 300 ml beaker; the cathode position was either vertical (**Fig. 2(a)**), facing a Pt mesh anode, or horizontal facing down (**Fig. 2(b)**), with the Pt mesh anode directly below. Growth experiments were performed using an EG&G potentiostat-galvanostat 263A at 50ºC; the temperature was maintained with a hot water jacket circulator. The electrolyte for morphological studies of Cu-Zn-Sn deposition was an alkaline solution containing 0.5M $K_4P_2O_7$, 10 mM $CuSO_4$, 60 mM $ZnSO_4$, and 5 mM $SnSO_4$ at pH 9.5. The deposition was performed for 7.5 minutes at -1.8V on Molybdenum foils with 1 cm2 active surface area. The films for compositional analysis instead were grown on Mo from a 0.2M $C_6H_8O_7$, 0.2M Na_2SO_4, 30mM $SnSO_4$, 30-45mM $ZnSO_4$, 40mM $CuSO_4$ electrolyte, with pH 2.3 for 35 seconds at -2.1VMSE on 0.5 cm^2 active surface area. The surface morphology of the Cu-Zn-Sn films was investigated with a FEI Quanta 650 SEM. Alloy composition was measured at nine distinct positions as shown in **Fig. 2** using an energy dispersive X-ray spectrometer with a 20 kV accelerating voltage.

3.2 Growth of Dendritic Structures in Different Electrode Orientations

A flat electrochemical cell was fabricated out of polypropylene; the internal volume consisted of a 3 cm x 8 cm x 0.8 cm channel into which two Cu plates were inserted as electrodes (**Fig. 3**). The channel was filled with a solution

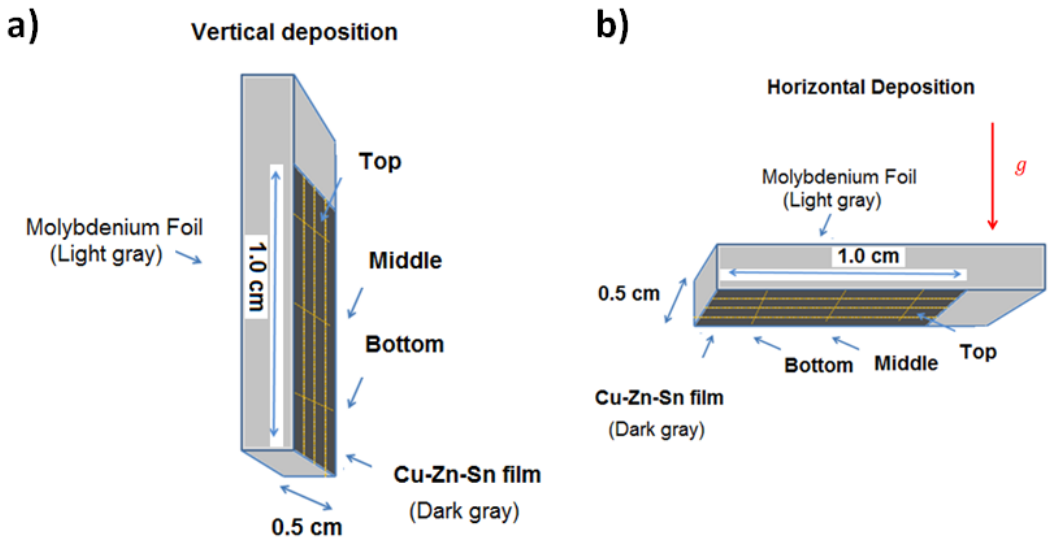

Fig. 2 Electrode set-up for Cu-Zn-Sn electrodeposition: a) vertical deposition set up and b) horizontal deposition set up (substrate facing down).

containing 0.1 M $CuSO_4$, providing a simple binary electrolyte for Cu electrodeposition. Upon addition of 5-10 mM $AgNO_3$ or 5-10 mM $NiSO_4$ Cu-Ag and Cu-Ni alloys could be grown, respectively. Electrodeposition was carried out at room temperature (25ºC) and under constant cell potential (a two-electrode configuration) of 20 or 40V applied with a Hewlett Packard DC power supply.

Visualization of growth was performed at 29 frames per second, with the images being captured by using a Sony A5100 camera fitted with a SMC Pentax-M 50 mm f/1.7 lens (Asahi Optical Corp.) at an aperture setting of f/5.6. Electrodeposition experiments were carried out over the course of 20 minutes. The four orientations examined were: cathode-top, cathode-bottom, channel flat, and channel horizontal (**Fig. 3**). Markers drawn on the cell were used to calibrate the length scales.

The frames from the video were extracted using FFMPEG 2.7.4, and the Python 2.7 libraries Pillow 3.0.0 + Numpy 1.10.4, Open CV 3.1.0, and Scikit-Learn 0.17. These were used for background subtraction, binarization of the image, and contour determination, respectively. ImageJ 1.49 (National Institutes of Health) was used to measure the offset angle to correct for the camera-captured image not being perfectly horizontal. In order to quantitatively measure the total area of the dendrites, the total number of pixels corresponding to the dendrite structure were summed. Similarly, in order to calculate the 1-D perimeter arclength of the dendrites, the total length of the contours detected by Scikit-Learn were summed.

4. Results and Discussion

4.1 Nucleation Features in Cu-Zn-Sn Alloys

The effect of geometry and gravity on electrochemical nucleation has been studied for various pure metals in refs.[7-10], showing clear differences in the morphological features and in some cases improved properties. In order to investigate the effect of gravity on alloy deposition we selected a Cu-Zn-Sn ternary alloy and plated films in a wide range of compositions. **Figure 4** shows the representative morphology of Cu-Zn-Sn films with

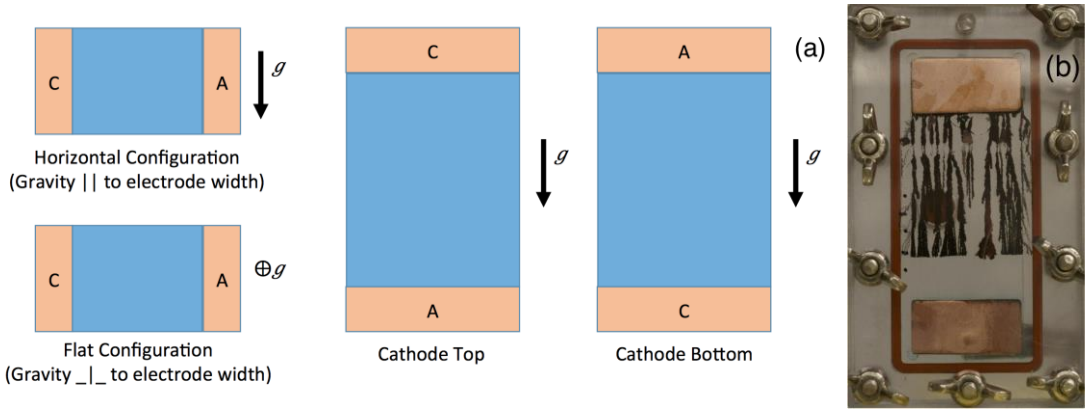

Fig. 3 (a) Schematic representation of electrode orientations explored for dendrite growth include channel horizontal, flat channel, cathode at the top, and cathode at the bottom. (b) Photograph of the cell after the growth of Cu-Ag dendrites. The black dots on the lower left of the cell are used for length calibration.

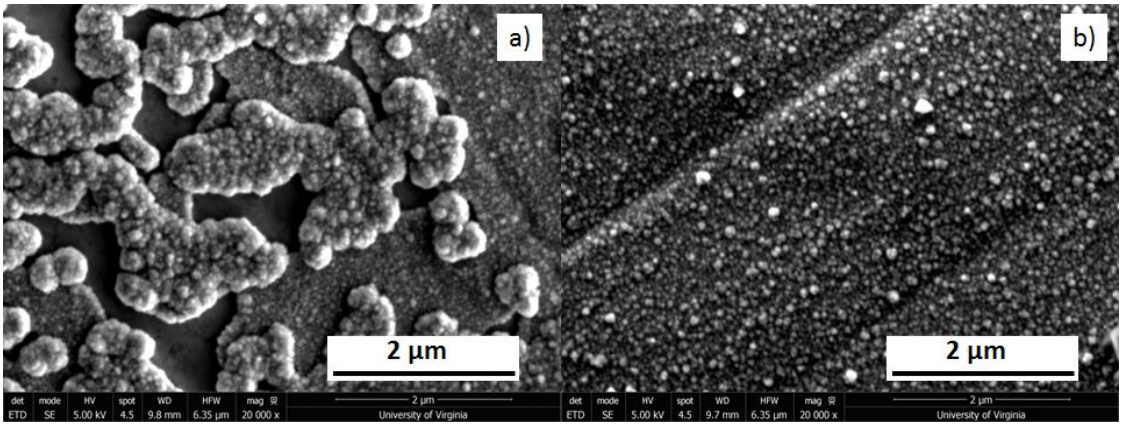

Fig. 4 Top down SEM images of films electrodeposited in a) vertical configuration and b) horizontal configuration for 7.5 minutes from an alkaline solution.

composition Cu 51 at%, Zn 24 at%, Sn 25 at% grown for 7.5 min, in the vertical (**Fig. 4(a)**) and horizontal (**Fig. 4(b)**) configuration. A significant improvement in the uniformity of the film during the initial stage of deposition is observed in the horizontal configuration, i.e. in the simulated absence of gravity. Morisue, et al.[16] discussed the effect of gravity on the electro-chemical nucleation of Cu on TiN; they found a lower number density of nuclei in the cathode over anode (C/A) configuration, vs. an anode over cathode (A/C) configuration. This has been related to a variation in the extent of the nucleation inhibition zone, giving a smaller nucleus size in the A/C configuration. We hypothesize that the irregular mounds found in the vertical configuration (**Fig 4(a)**) may be originated by clustering of closer nuclei, as well as by irregularities in the thickness of the diffusion layer and the flow patterns due to the natural convection that exist in the vertical configuration.

4.2. Compositional Uniformity

On similar films, grown however from a citrate based acidic solution, we have quantified the spread of composition in ternary Cu-Zn-Sn alloys grown in a vertical vs. a horizontal cell configuration. **Figure 5** reports the compositional distribution of Cu and Zn fraction in the alloy after growth at 76 mA/cm^2, in conditions otherwise identical. The average spread in composition for the vertical configuration is 1.7 at% for both Cu and Zn; in the horizontal configuration instead a 0.7 at% for Cu and 0.9 at% spread for Zn, respectively, is measured. The compositional variation is half as much in the horizontal configuration, suggesting that the decrease in the extent of natural convection is at the origin of the improved uniformity. Note that the compositional trend for Cu and Zn in the vertical direction is approximately monotonous (increasing with height for Cu, decreasing with height for Zn), suggesting that the changes in composition may be related at least in part to the variation of the diffusion layer thickness δ generated by natural convection, which has been determined to follow a δ ~ x1/5 dependence, where x is the height[17]. It should be noted however that the calculated limiting diffusion partial currents for Cu, Zn and Sn give a total limiting current of the order of 5 mA/cm^2, much lower than the total applied current of the order of 76 mA/cm^2; the

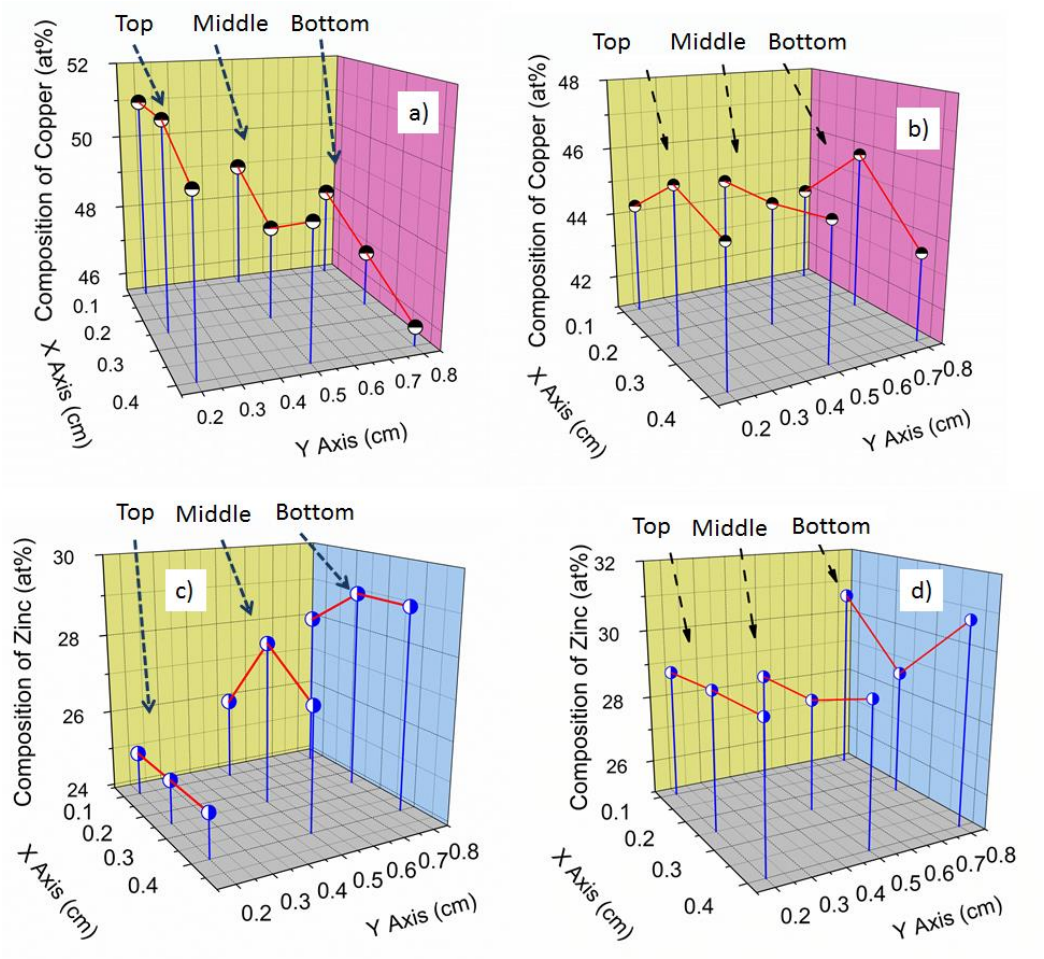

Fig. 5 Comparison of compositional distribution across a 1 cm x 0.5 cm sample in a vertical configuration (left) and a horizontal configuration, cathode on top (right), of copper and zinc.

remainder of the current is most probably due to hydrogen reduction, suggesting that the compositional trends in the vertical direction may therefore be affected by the evolution of hydrogen during deposition.

4.3 Dendritic Growth of Alloys from a Binary Electrolyte

Previous work by Bockris[18], and Fukunaka and Rosso[7,19] have identified three flow regimes in microgravity and have shown the onset of dendrites formation at the transition time, i.e. the time at which the metal ion concentration at the electrode approaches zero. No clear understanding of dendritic growth in alloys has been achieved until now; we investigate this aspect by comparing the dendritic growth of metals and alloys in various configurations, under gravity and in simulated microgravity conditions.

4.3.1 Deposition of Cu and Cu Alloy Dendrites

The growth of Cu, Cu-Ag and Cu-Ni dendrites in different electrode orientations was investigated by performing electrodeposition in a thin-channel cell as described in the experimental section. **Figure 6** shows the effect of increasing voltage on a cell with both electrode plates vertical, the cathode on the left side, and gravity pointing downward in the image. The growth of dendrites is biased towards the top of the cell, propagating in the clockwise direction; this evidences the occurrence of natural convection as shown in **Fig. 1**. This flow occurs upwards at the left due to the decrease in electrolyte density in proximity of the cathode. **Figure 7** shows the growth of dendrites at 20V in different orientations. When the cathode is at the top of the cell (**Fig. 7(a)**), the dendrites grow as aligned, approximately columnar structures. In this case, metal reduction at the top causes the lighter fluid formed in the upper region to be compressed there[20]; the diffusion of metal ions towards the deposit therefore is hindered. Growth instability results in straight, columnar dendrites; this configuration leads to inhibition of the

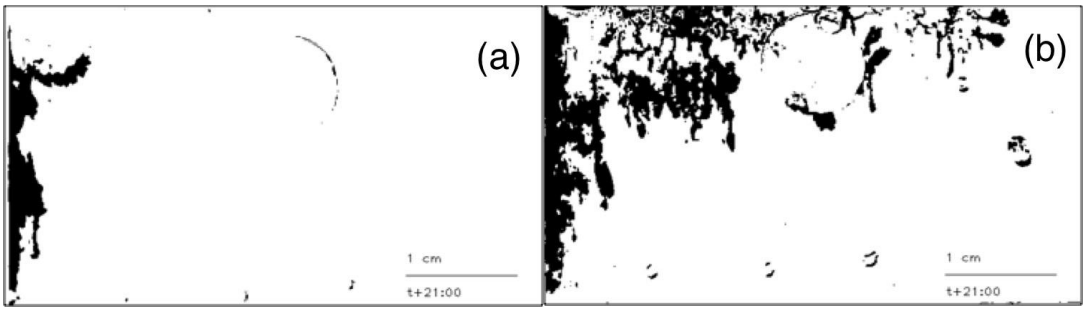

Fig. 6 Growth of dendritic structures in 0.1 M $CuSO_4$ for 20 minutes at vertically oriented electrodes ($\boldsymbol{g}\downarrow$); orientation biases the growth of the dendrites towards the top of the cell (a, 20V; b, 40V). Increasing the voltage accelerates growth of the dendrites.

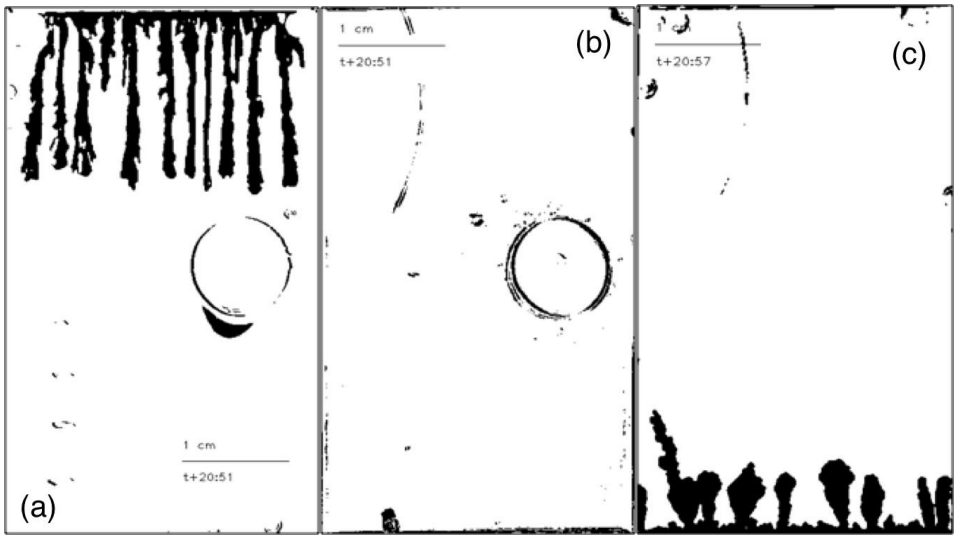

Fig. 7 Growth of dendritic structures in 0.1M $CuSO_4$ for 20 minutes at 20V in (a) Top cathode ($\boldsymbol{g}\downarrow$) configuration showing growth of aligned columns of dendrites, (b) bottom cathode ($\boldsymbol{g}\downarrow$) configuration showing suppressed growth of dendrites, and (c) channel in flat configuration ($\boldsymbol{g}\oplus$) showing a coarse branching dendritic structure.

growth of side branches due to the highly directional arrival of ions to the growing stems.

With the cathode at the bottom (**Fig. 7(b)**), the electrolyte becomes lighter in the bottom region, and natural convection is enhanced. Turbulent flow ensues and the dendrites being formed tend to be fractured and dispersed in the cell, seemingly leading to complete suppression of the dendrite growth. Finally, when the electrodes are placed in a channel flat configuration with gravity perpendicular to the plane of the image (**Fig. 7(c)**), the growth of the electrodes takes on a coarse branching with splitting fingers, leading to non-aligned dendrite structures.

The effect of adding 5-10 mM Ag+ to the Cu electrolyte on the growth of dendrites from a cathode-top configuration at 20V is shown in **Fig. 8**. In this case, under the assumption of deposition under diffusion limiting conditions, we estimate that the deposit consists of Cu-Ag with 5-10 at % Ag, respectively. The growth morphology consists of straight columns with relatively high density and increasing width as growth progresses, probably due to tip-splitting events. While the length of the dendrites is

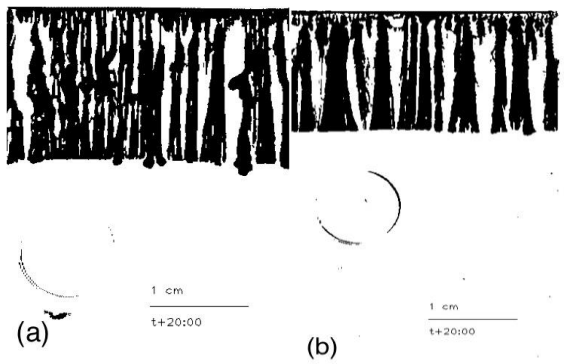

Fig. 8 Growth of dendritic structures in a cathode top ($\boldsymbol{g}$ ↓) configuration from a solution containing 0.1 M $CuSO_4$ at 20V for 20 minutes with the addition of (a) 5 mM AgNO3 and (b) 10 mM AgNO3. The addition of Ag does not appreciably affect the length of the dendrites, but they are more densely packed.

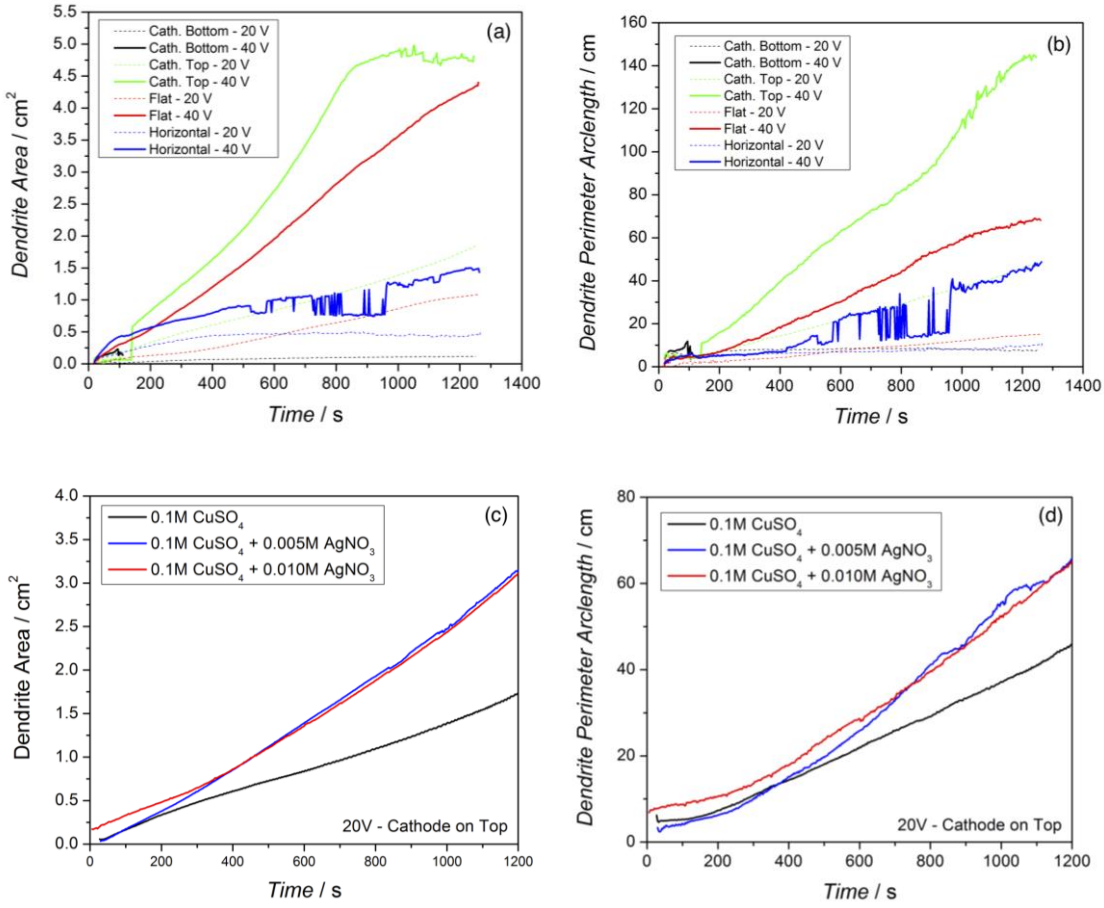

Fig. 9 Area (a, c) and perimeter arclength (b, d) of dendrites grown in different orientations and with various voltages. (a) and (b) show the evolution of dendrite area and perimeter for Cu deposition in various geometries; (c, d) show the effect of the addition of Ag for the cathode on top configuration, 20 V, which increases both surface area and perimeter arclength.

approximately the same in the Cu-Ag as the Cu dendrites in **Fig. 7(a)**, the density and the surface area are both higher. An increase in dendrite density in pure metals is usually observed at higher applied voltages[21], due to the higher probability of re-nucleation and therefore the increased chance of geminating side branches. We show here that a similar effect can be obtained in alloys without increasing the applied voltage. We hypothesize that accommodation of the reducing foreign atoms (Ag) in the host lattice structure (Cu) is hindered by the difference in atomic volume between Cu and Ag, ~ 13 %. This would result in phase separation between Cu and Ag, and/or in re-nucleation instead of continued grain growth, thus resulting in additional branches which densify the deposit.

The previous findings have thus far been mostly qualitative. In order to obtain a quantitative description of the growth and morphology of these dendritic structures, image analysis was performed to measure the 2-D apparent area of the dendrites and the 1-D surface arclength. **Figure 9** summarizes these parameters for the various deposition geometries during Cu deposition and upon addition of Ag ions. The results of the analysis demonstrate that the highest dendrite area and surface arclength in Cu deposition are ranked in the following order: Cathode-Top > Channel Flat > Channel Horizontal > Cathode-Bottom. Growth of the dendrites from the top cathode is limited by the mechanical strength of the structures: as the deposition time exceeds 800 seconds for the 40 V condition, fragments of the dendrites begin to break off and the increase in area shown in **Fig. 9(a)** is arrested. Note that the dendrite area and perimeter arclength in the cathode on top configuration increases suddenly at about 130 s, due to an induction time delay. In the horizontal configuration, 40 V, instead the oscillations in the data are due to the periodic break-up of the dendrites. Upon the addition of Ag, the total 2-D area and 1-D surface arclength are observed to double and increase by a factor of 50 %, respectively. Changing the concentration of $AgNO_3$ in the electrolyte however, has no observable effect on these two parameters, probably as a consequence of the limited increase in Ag fraction in the deposit.

The addition of 5-10 mM $NiSO_4$ to the 0.1 M $CuSO_4$ solution results in the formation of Cu-Ni deposits with an estimated Ni fraction of 5-10 at %. At variance with the Cu-Ag system, the Cu-Ni system tends to form a continuous series of solid solutions. The addition of Ni leads to thinner and more dense dendritic structures, a tendency that increases with the Ni concentration in solution (**Fig. 10**). Ni is known to be reduced at high overpotentials, resulting in a higher nucleation probability and therefore smaller grains; the above observation therefore could be interpreted in terms of a finer microstructure, i.e. denser branches. It should be noted that a higher Ni content leads to seemingly dense (at the cm level) columns. Similar features are observed for a flat channel configuration (**Fig. 11**). **Figure 11** should be compared to **Fig. 7(c)**, where the Cu dendritic structure are

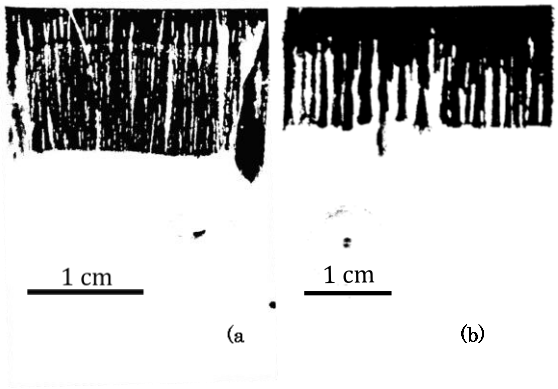

Fig. 10 Growth of dendritic structures in a top cathode ($\boldsymbol{g}\downarrow$) configuration from a solution containing 0.1 M $CuSO_4$ at 20V for 20 minutes with the addition of (a) 5 mM $NiSO_4$ and (b) 10 mM $NiSO_4$.

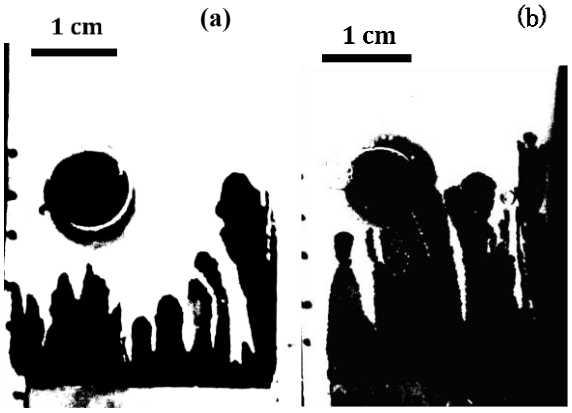

Fig. 11 Growth of dendritic structures in a channel flat configuration ($\boldsymbol{g}\oplus$) formation from a solution containing 0.1 M $CuSO_4$ at 20V for 20 minutes with the addition of (a) 5 mM $NiSO_4$ and (b) 10 mM NiSO4.

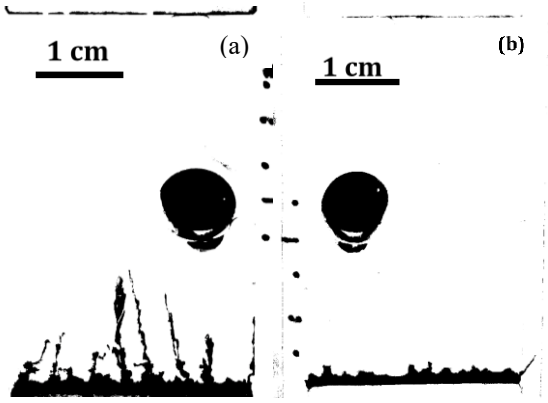

Fig. 12 Growth of dendritic structures in a cathode bottom ($\boldsymbol{g}\downarrow$) configuration from a solution containing 0.1 M $CuSO_4$ at 20V for 20 minutes with the addition of (a) 5 mM $NiSO_4$ and (b) 10 mM $NiSO_4$.

branched. Ni additions in this case also results in more dense features, seemingly approaching fully dense deposits. Morphological differences between pure Cu and Cu-Ni alloys are also observed in the bottom cathode configuration (**Fig. 12**); at 20 V with 5 mM Ni^{2+} thin fingers are seen, showing in some cases tip splitting; with 10 mM Ni^{2+} instead formation of such fingers is inhibited, suggesting a tendency to the formation of a thin, dense and compact film. The latter observations could also be explained in terms of removal of the dendrites by the convection flow, as seen for pure Cu; we assume however that the addition of Ni would enhance the mechanical properties of the dendrites, limiting fracturing.

5. Conclusion

The ability to control the geometrical features, composition and morphology of electrochemically grown metallic films and micro/nano structures is key to the enhancement of device performance and their versatility. Advances in this field require a better understanding of electrochemical deposition of metals and alloys in ideal conditions, specifically in absence of natural convection phenomena; this may be achieved by low gravity experiments or by utilizing cell geometries where natural convection is inhibited. This work demonstrates that alloy electrodeposition in a geometry conducive to suppression of natural convection (cathode on top) provides for an improved uniformity of film morphology and film composition. Additionally, it is shown that the effect of alloying Ag or Ni (5-10 at %) to dendritic Cu results in significant morphology changes, including a higher dendrite density and enhanced branching with smaller features. It is hypothesized that Ag additions induce branching due to the difference in atomic volume and its immiscibility with Cu, while Ni decreases feature size due to the high overvoltage needed for reduction, leading to a higher nucleation rate.

Acknowledgements

This work was partly supported through the awards NSF CMMI 1131571.

Reference

1) Y.D. Gamburg and G. Zangari: Springer Science & Business Media, Theory and practice of metal electrodeposition (2011).
2) M. Schlesinger and M. Paunovic P. Milan: eds., Modern electroplating, John Wiley & Sons, **55** (2011).
3) G. Zangari: Electrochemical Society Interface, **31** (2011).
4) G. Zangari: Coatings 5, **2** (2015) 195.
5) J. Newman and K.E. Thomas-Alyea, T.A. Karen, E.: Electrochemical systems, 3rd ed., John Wiley & Sons (2012).
6) A. Ehrl, B. Georg, G. Volker and A.W. Wolfgang: J. of Computational Physics, **235** (2013) 764.
7) K. Nishikawa, Y. Fukunaka, E. Chassaing and M. Rosso: J. of Physics, Conference Series, **327** (2011) 012045, IOP Publishing.
8) Y. Fukunaka, K. Okano, Y. Tomii, Z. Asaki and K. Kuribayashi: J. of the Electrochemical Society, **145** (1998) 1876.
9) C. Riley and H.D. Coble: Final Report, NASA Contract NAS8-33812 (1982).
10) G.W. Maybee, R. Clyde and H.D. Coble: NASA Get Away Special Experimenter's Symposium, Goddard Space Flight Center, Greenbelt, MD., (1986).
11) H.A. Laitinen and I. M. Kolthoff: J. of the American Chemical Society, **61**.(1939) 3344.
12) A.J. Bard and R.F Larry: Electrochemical methods, fundamentals and applications,. New York, Wiley, (1980).
13) K.J. Vetter: Electrochemical kinetics, theoretical aspects. Elsevier, (2013).
14) D. Landolt: Plating and surface finishing, **88** (2001) 70.
15) S.R. Brankovic and G. Zangari: Electrochemical Engineering Across Scales, From Molecules to Processes, **15** (2015).
16) M. Morisue, Y. Fukunaka, E. Kusaka, R. Ishii and K. Kuribayashi: J. of Electroanalytical Chemistry, **559** (2003) 155.
17) Y. Awakura and Y. Kondo: J. of The Electrochemical Society, **123** (1976) 1184.
18) J.L Barton and JO'M. Bockris: Proceedings of the Royal Society of London A, Mathematical, Physical and Engineering Sciences, The Royal Society, **268** (1962) 485.
19) K. Nishikawa, Y. Fukunaka, E. Chassaing and M. Rosso: Electrochimica, Acta, **100** (2013) 342.
20) F. Argoul, G. Gadret, C. Léger and F. Texier: European Space Agency-Publications, ESA SP, **385** (1996) 259.
21) L.L-Tomas, J. Mach, P.P. Trigueros, F. Mas, J. Claret and F. Sagues: Chaos, Solitons & Fractals, **6** (1995) 287.

.